[논문] 한국소성가공학회지, 제 14 권 제 6 호, 2005
Transactions of Materials Processing, Vol.14, No.6, 2005

얇은 판상의 석출을 포함한 결정의 초기항복응력 이방성 및 경화거동에 관한 모델링

김준형[1]· 한정석[2]· 정관수#· 강태진[1]

Modeling the Anisotropy of Initial Yield Strength and Hardening Behavior of Crystals with Thin Platelet Precipitates

J. H. Kim, C. S. Han, K. Chung, T. J. Kang

(Received May 12, 2005)

Abstract

Precipitates, present in most commercial alloys, can have a strong influence on strength and hardening behavior of a single crystal. The effect of thin precipitates on the anisotropy of initial slip resistance and hardening behavior of crystals is modeled in this article. For the convenience of the computational derivation and implementation, the material formulation is given in the unrotated intermediate configuration mapped by the plastic part of the deformation gradient. Material descriptions for the considered two phased aggregates consisting in lattice hardening as well as isotropic hardening and kinematic hardening are suggested. Numerical simulations of various loading cases are presented to discuss and assess the performance of the suggested model. From the results of the numerical simulation, it is found that the suggested model represents the initial plastic anisotropy at least qualitatively well and that it has an improved representation of various characteristic hardening behaviors in comparison with conventional hardening descriptions where the precipitate structure is not reflected.

Key Words: Crystal plasticity, Particulate reinforced materials, Hardening, Finite Elements

1. Introduction

Precipitation strengthening is one of classical approaches to enhance the initial strength and hardening behavior of metals. The influences of precipitates on the mechanical characteristics of crystals and in metallic alloys have been investigated by various authors [1-4]. From these investigations, it is known that the size, shape, spacing and orientation of precipitates, which can be altered during aging processes, have a strong influence on the plastic behavior. While precipitates can influence the initial yield strength and its anisotropy, they can also dominate the hardening behavior, in particular, control kinematic hardening effects. With the influence which precipitates have on single crystals, corresponding effects on the anisotropy of widely applied polycrystalline materials with precipitates can be expected. In this context, it is desirable to establish an elaborate model which can represent the effect of precipitates on the plastic anisotropy of initial yield strength as well as the isotropic hardening and kinematic hardening on single crystals. In this paper, the effect of thin precipitates on

1. 서울대학교 재료공학부
2. Max-Planck-Institut fuer Eisenforschung
교신저자: 서울대학교 재료공학부
E-mail: kchung@snu.ac.kr

Table 1 Kinematic relations, stress/strain expressions and governing relations in the intermediate configuration $\widetilde{B}$ in crystal plasticity

Multiplicative decomposition	$\mathbf{F}=\mathbf{F}_e\mathbf{F}_p$	(1)
velocity gradient	$\mathbf{l}=\mathbf{l}_e+\mathbf{F}_e\widetilde{\mathbf{L}}_p\mathbf{F}_e^{-1}$	(2)
	with $\mathbf{l}_e=\dot{\mathbf{F}}_e\mathbf{F}_e^{-1}$ and $\widetilde{\mathbf{L}}_p=\dot{\mathbf{F}}_p\mathbf{F}_p^{-1}$	(3)
Plastic velocity gradient	$\widetilde{\mathbf{L}}_p=\sum_\alpha\dot{\gamma}^\alpha(\tilde{\mathbf{s}}^\alpha\otimes\tilde{\mathbf{m}}^\alpha)=\widetilde{\mathbf{D}}_p+\widetilde{\mathbf{W}}_p$	(4)
	$\widetilde{\mathbf{D}}_p=\sum_\alpha\dot{\gamma}^\alpha(\tilde{\mathbf{s}}^\alpha\otimes\tilde{\mathbf{m}}^\alpha)_s$	(5)
	$\widetilde{\mathbf{W}}_p=\sum_\alpha\dot{\gamma}^\alpha(\tilde{\mathbf{s}}^\alpha\otimes\tilde{\mathbf{m}}^\alpha)_a$	(6)
Lagrangian strain tensor	$\widetilde{\mathbf{E}}=\frac{1}{2}(\mathbf{F}_e^T\mathbf{F}_e-\mathbf{F}_p^{-T}\mathbf{F}_p^{-1})=\widetilde{\mathbf{E}}_e+\widetilde{\mathbf{E}}_p$	(7)
	$\widetilde{\mathbf{E}}_e=\frac{1}{2}(\mathbf{F}_e^T\mathbf{F}_e-\mathbf{1})$	(8)
	$\widetilde{\mathbf{E}}_p=\frac{1}{2}(\mathbf{1}-\mathbf{F}_p^{-T}\mathbf{F}_p^{-1})$	(9)
Second Piola-Kirchhoff stress	$\widetilde{\mathbf{S}}=\mathbf{F}_e^{-1}\boldsymbol{\tau}\mathbf{F}_e^{-T}$	(10)
Mandel stress	$\widetilde{\mathbf{P}}=(\mathbf{1}+2\widetilde{\mathbf{E}}_e)\widetilde{\mathbf{S}}=\widetilde{\mathbf{C}}_e\widetilde{\mathbf{S}}$	(11)
Isotropic relation	$\widetilde{\mathbf{S}}=\widetilde{\boldsymbol{\Gamma}}_e\widetilde{\mathbf{E}}_e$	(12)
Resolved shear stress	$\tau^\alpha=\widetilde{\mathbf{P}}\cdot(\tilde{\mathbf{s}}^\alpha\otimes\tilde{\mathbf{m}}^\alpha)_s$	(13)
Yield function	$\Phi^\alpha=\lvert\tau^\alpha-x^\alpha\rvert-g^\alpha$	(14)
Kuhn-Tucker-type conditions	$\mathrm{sgn}(\tau^\alpha-x^\alpha)\dot{\gamma}^\alpha\geq 0\quad\Phi^\alpha\leq 0$, $\dot{\gamma}^\alpha\Phi^\alpha=0$	(15)

the anisotropy of the initial slip resistance, the isotropic hardening and the kinematic hardening is modeled and numerical simulations are performed.

2. Notations and constitutive setting

Kinematic relations, stress/strain-expressions and governing relations in the intermediate configuration $\widetilde{B}$ in the conventional crystal plasticity are summarized in

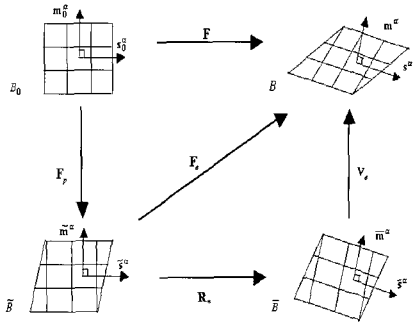

Fig. 1 Intermediate configurations obtained by $\mathbf{F}=\mathbf{F}_e\mathbf{F}_p=\mathbf{V}_e\mathbf{R}_e\mathbf{F}_p$

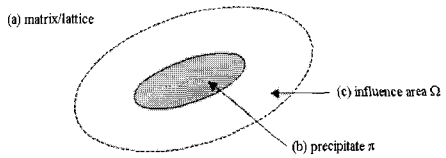

Fig. 2 Influence area Ω around a precipitate π

the Table 1. Therein, the decomposition (1) of deformation gradient $\mathbf{F}$ into elastic $\mathbf{F}_e$ and plastic part $\mathbf{F}_p$ is applied, where it is assumed that the rotation of the lattice is contained in $\mathbf{F}_e$ (see Fig. 1). The plastic velocity gradient can be expressed with (4), where $\dot{\gamma}^\alpha$ denotes the plastic shearing rate, $\tilde{\mathbf{s}}^\alpha$ the slip direction and $\tilde{\mathbf{m}}^\alpha$ the slip plane normal of slip system α in $\widetilde{B}$ with $|\tilde{s}^\alpha|=|\tilde{m}^\alpha|=1$ and $\tilde{\mathbf{s}}^\alpha\cdot\tilde{\mathbf{m}}^\alpha=0$.

3. Evolution equations for the hardening

In view of Fig. 2, the resolved shear stress is divided into three parts: the average resolved shear stress of the lattice τ_M^α, the average stress in the influence region τ_Ω^α weighted with the relevant area fraction ω and the average of the stress within the inclusion τ_I^α weighted with the relevant volume fraction f, yielding

$$\tau^\alpha=(1-f-\omega)\tau_M^\alpha+\omega\tau_\Omega^\alpha+f\tau_I^\alpha. \tag{16}$$

For incorporation of such a model with the internal variable approach, the different stress components weighted with their area and volume fractions are

$$\hat{\tau}_\Omega^\alpha=\omega(\tau_\Omega^\alpha-\tau_M^\alpha)\quad\text{and}\quad\hat{\tau}_I^\alpha=f(\tau_I^\alpha-\tau_M^\alpha) \tag{17}$$

yielding

$$\tau^\alpha=\tau_M^\alpha+\hat{\tau}_\Omega^\alpha+\hat{\tau}_I^\alpha. \tag{18}$$

The influence area ω may be dependent on the size of the precipitate. For simplicity, however, it is assumed that ω is proportional to f, which yields both hardening components $\hat{\tau}_{\Omega}^{\alpha}$ and $\hat{\tau}_{I}^{\alpha}$ to be proportional to f in (17).

As correspondence to the internal variables applied in (14), it is suggested to correlate the slip resistance to the hardening mechanisms of the matrix $g^{\alpha} = \tau_{M}^{\alpha} + \hat{\tau}_{\Omega}^{\alpha}$ and, following Bate et al. [2], the back stress to the stress in the precipitate, as $x^{\alpha} = \hat{\tau}_{I}^{\alpha}$. In average, the elastic range and thus also the back stresses are assumed to be small in Ω and negligible in the matrix area. In the following the kinematic hardening related to Ω is, as for other regions of the lattice, neglected.

Thin precipitates, considered here, like the θ' precipitates, are normally aligned parallel to the habit planes (see Fig. 3) after the aging process. The volume fraction of each habit plane can vary depending on the aging process. In the deformation process of the aggregate, the inhomogeneous deformation is in part accommodated by rotations of the precipitates relative to the lattice (see Fig. 4).

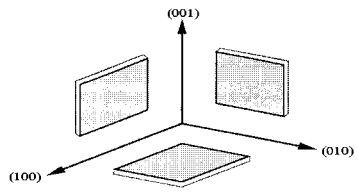

Fig. 3 Precipitates in habit planes

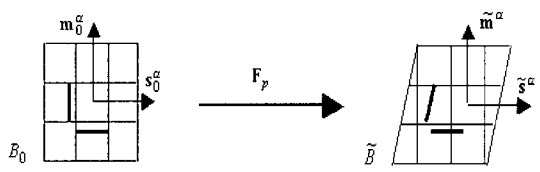

Fig. 4 Rotation of precipitates by $\mathbf{F}_p$

All hardening descriptions of the suggested material model are summarized in Table 2. In Table 2, the fourth order tensor $\tilde{\mathbf{H}}^{\pi}$ is defined as

$$\tilde{\mathbf{H}}^{\pi} = \sum_{ijkl}^{3} H_{ijkl}^{\pi}\, \tilde{\mathbf{e}}_i^{\pi} \otimes \tilde{\mathbf{e}}_j^{\pi} \otimes \tilde{\mathbf{e}}_k^{\pi} \otimes \tilde{\mathbf{e}}_l^{\pi} \qquad (19)$$

Table 2 Hardening descriptions for a single crystal with thin precipitates

Slip resistance

$$\dot{g}^{\alpha} = \sum_{\beta} \left(h_M^{\alpha\beta} + h_{\Omega}^{\alpha\beta} \right) \left| \dot{\gamma}^{\beta} \right| \qquad (20)$$

Work hardening moduli of the lattice

$$h_M^{\alpha\beta} = [q_M + (1 - q_M)\delta^{\alpha\beta}] h_M^{\beta} \qquad (21)$$

$$h_M^{\beta} = \tau_M^0 \left(\frac{c_M \gamma}{b_M \tau_M^0} + 1 \right)^{b_M} \qquad (22)$$

Moduli related to the hardening induced by precipitates

$$h_{\Omega}^{\alpha\beta} = [q_M + (1 - q_M)\delta^{\alpha\beta}] h_{\Omega}^{\beta} \qquad (23)$$

$$h_{\Omega}^{\alpha} = \frac{1}{f} \sum_{\pi} f^{\pi} h_{\Omega}^{\pi\alpha} \sqrt{(\tilde{\mathbf{s}}^{\alpha} \otimes \tilde{\mathbf{m}}^{\alpha})_S \cdot \tilde{\mathbf{H}}^{\pi} (\tilde{\mathbf{s}}^{\alpha} \otimes \tilde{\mathbf{m}}^{\alpha})_S} \qquad (24)$$

$$h_{\Omega}^{\pi\alpha} = h_{\Omega}^{o} \sec \mathrm{h}^2 \left(\frac{h_{\Omega}^{o} \gamma}{\tau_{\Omega}^{S} - \tau_{\Omega}^{o}} \right) \qquad (25)$$

Kinematic hardening induced by precipitates

$$\hat{\tau}_I^{\alpha} = x^{\alpha} = \tilde{\mathbf{C}}_e \tilde{\mathbf{X}} \cdot (\tilde{\mathbf{s}}^{\alpha} \otimes \tilde{\mathbf{m}}^{\alpha})_S \qquad (26)$$

$$\tilde{\mathbf{X}}^{\nabla} = c_x f \tilde{\mathbf{\Gamma}}_e \tilde{\mathbf{H}} \sum_{\beta} \dot{\gamma}^{\beta} (\tilde{\mathbf{s}}^{\beta} \otimes \tilde{\mathbf{m}}^{\beta})_S - b_x \left| \dot{\gamma} \right| \tilde{\mathbf{X}} \qquad (27)$$

$$\tilde{\mathbf{H}} = \frac{1}{f} \sum_{\pi} f^{\pi} \tilde{\mathbf{H}}^{\pi} \qquad (28)$$

with the base vectors of the precipitates $\tilde{\mathbf{e}}_i^{\pi}$. The components of $\tilde{\mathbf{H}}^{\pi}$ can be given with $H_{ijkl}^{\pi} = 1$ for $i=j=k=l$, $(i, j, k, l)=(2, 3, 2, 3)$, $(i, j, k, l)=(3, 2, 3, 2)$ and otherwise $H_{ijkl}^{\pi} = 0$ for a platelet precipitate aligned to [100] plane and $\tilde{\mathbf{e}}_i^{\pi}$ parallel to (100), (010), and (001), respectively. The expressions for $\tilde{\mathbf{H}}^{\pi}$ aligned to other habit planes are then obtained by rotation of $\tilde{\mathbf{e}}_i^{\pi}$, $i = 1, 2, 3$.

4. Numerical examples

The numerical algorithm has been implemented into the ABAQUS explicit material user interface[5] and all simulations have been performed explicitly. The step

Table 3 Material parameters of the Al-Cu single crystal

Young's modulus $E = 70000$ MPa	$q_\Omega = 1.4$
Poisson's ratio $\nu = 0.3$	$h_\Omega^o = 135$ MPa
$q_M = 1.4$	$\tau_\Omega^o = 60$ MPa
$\tau_M^o = 0.98$ MPa	$\tau_\Omega^S = 100$ MPa
$b_M = 0.4$	$b_x = 30.0$
$c_M = 784$ MPa	$c_x = 2.0$
$\tau_{Mo}^\alpha = 10$ MPa	$s_{\Omega o}^\pi = 50$ MPa
$f = 0.03$ *	

*This value is used for all the simulations unless otherwise noted as for Table 4.

sizes have been chosen in such a way that the kinetic energy is negligible compared to the strain energy. The material parameters applied in the following examples are given in Table 3 if not otherwise noted in the text. The values of material parameters are referred from Han et al [6].

4.1 Initial yield

To illustrate the plastic anisotropy in the initial yield of the suggested model, tensile deformation of Al-xCu crystals with different microstructures are considered. To illustrate the performance of the proposed approach, numerical calculations have been preformed and results in the initial yield stress were compared with experimental results obtained by Zhu et al. [4] and predictions listed therein obtained by the models suggested in Hosford & Zeisloft [1] and Bate et al. [2]. As shown in Table 4, our proposed model yields closer results to those obtained experimentally than the models of Hosford & Zeisloft [1] and Bate et al. [2].

4.2 Monotonous loading

The performance of the suggested model in the hardening behavior for monotonous loading will be discussed next by considering tensile compression tests. Simulations are performed using a single eight-node continuum element under homogeneous deformation. Simple stretch directions are aligned to the element edges and all faces remain parallel to the initial configuration. A volume fraction of f =0.03 and a equally distribution of the precipitates along the habit planes [100], [010] and

Table 4 Comparison between experimental and simulation results for the modified axial component of the initial yield stress, τ_{axial} in the stress-free-aged and stress-aged Al-Cu specimens

Specimen number	Experimental results*		Simulation results		
	τ_{axial}^{ex} (Mpa)	δ^{ex} (%)	δ	δ^{H} **	δ^{B} ***
1f	80	-15.3	-7.9	-6.1	-33.6
1s	67.8				
2f	78	-13.1	-7.7	-17.1	-26.5
2s	67.8				
3f	79.2	-12.4	-7.7	-7.9	-31.9
3s	69.4				
4f	68.6	-12.0	-7.5	2.1	-41.8
4s	60.4				
5f	67.8	-22.3	-7.4	-3.4	-36.4
5s	52.7				
6f	63.7	-3.9	-3.6	1.2	21.9
6s	61.2				

* Data from Zhu et al. [4]
** δ^{H} : predicted by Hosford's plastic inclusion model
*** δ^{B} : predicted by Bate's elastic inclusion model

[001] is assumed. For comparison additional simulations with a conventional hardening model, e.g. Chang & Asaro [7], have been performed where the precipitate substructure is not taken into account. Material parameters of this conventional model are fitted in such a way that the stress-strain behavior in [100][010][001] orientation of both models have a similar behavior (see Fig. 5).

The determining material parameters of the conventional model, as explained above, are listed in Table 5. In Fig. 6 the compressive stresses over the compressive strain in various crystalline orientations are illustrated where the anisotropy of the hardening behavior is reduced in the predictions of the suggested material model considering the precipitate substructure. In this respect it should be noted that in comparison to pure Al-crystals, a reduced anisotropic hardening behavior was reported in experiments for alloys containing θ' precipitates (Hosford & Zeisloft [1]).

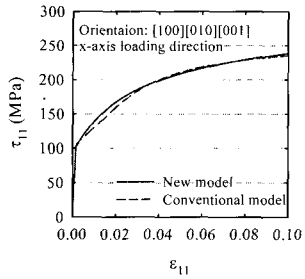

Fig. 5 τ_{11} versus ε_{11} in [100] orientation without (conventional model) and with precipitates (new model)

Table 5 Material parameters for the conventional model*

g_o^α	q	h_o	τ_s	τ_o
41MPa	1.4	600MPa	104MPa	60MPa

*Model of Chang & Asaro [6]: slip resistance $g^\alpha = \sum_\beta h_g^{\alpha\beta} |\dot{\gamma}^\beta|$,

$h_g^{\alpha\beta} = [q + (1-q)\delta^{\alpha\beta}]h_g^\beta$ and $h_g^\beta = h_o \mathrm{sech}^2\left(\frac{h_o \gamma}{\tau_s - \tau_o}\right)$

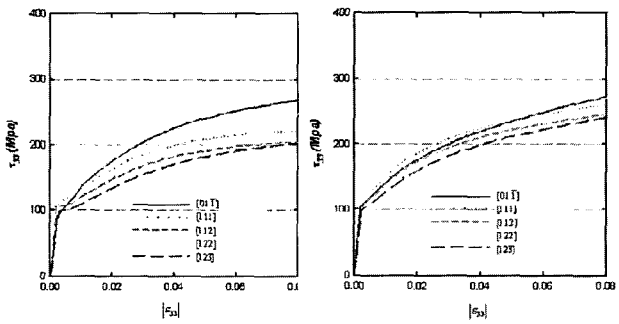

Fig. 6 τ_{33} versus ε_{33} in various orientations without (left) and with (right) precipitates

In the above considerations homogeneous deformation was assumed which may not be present in experimental tests. Even for simple compression tests, local lattice rotations from boundary constraints arise yielding inhomogeneous deformation. As a result, a homogeneous single crystal can transform into a multi-crystal at higher strains. Therefore, simulations of experimental tests have to be performed with more than one element to capture the real deformation process.

As an example, a circular cylinder with radius 5mm and height 5mm is considered. The bottom plane is fixed in vertical z-direction and the top plane is moved down for the simple compression test case. The number of element is 1456. To illustrate the inhomogeneous deformation, the equivalent plastic strain according to the corresponding compressive logarithmic strain ε_{33} for the $[122][2\bar{1}0][24\bar{5}]$ crystalline orientation is given in Fig. 7. Local lattice rotations yield the inhomogeneous deformation, since the material at the top and bottom can not rotate as in the interior. The inhomogeneity increases with the deformation, which can be seen by the minimum and maximum values of the equivalent plastic strain, starting with min/max strains of 0.08981 and 0.1447 at $\varepsilon_{33} = -0.05$ to 0.6345 and 1.654 at $\varepsilon_{33} = -0.35$. As a consequence, the orientation of the single crystal can be considered to change locally, as it has been also observed experimentally and numerically in Becker et al. [8].

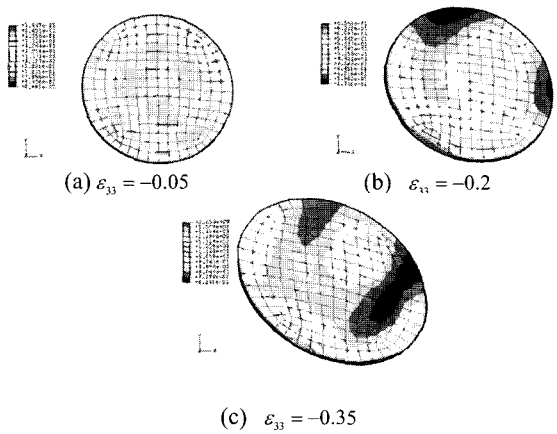

Fig. 7 Accumulated shear strain γ versus ε_{33}

4.3 Back stress and non-monotonous loading

Materials with precipitates are known to exhibit strong Bauschinger effects which are accounted for by back stresses in the material description. In Fig. 8 strains versus stresses in tension-compression in different directions are illustrated, showing the differences in kinematic hardening. Fig. 9 shows stress-strain diagrams where the material is first deformed in x_1-direction and then in the x_2-direction. While the $[122][2\bar{1}0][24\bar{5}]$ orientation is hardly affected by the precipitate rotation the $[1\bar{1}0][001][\bar{1}\,\bar{1}0]$ orientation shows quite considerable differences in the hardening behavior applying the precipitate rotation or not.

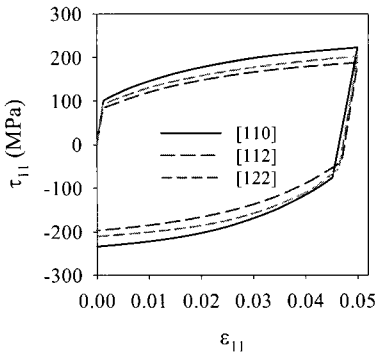

Fig. 8 Tensile and reverse stresses (τ_{11}) versus ε_{11} in [110], [112] and [122] direction

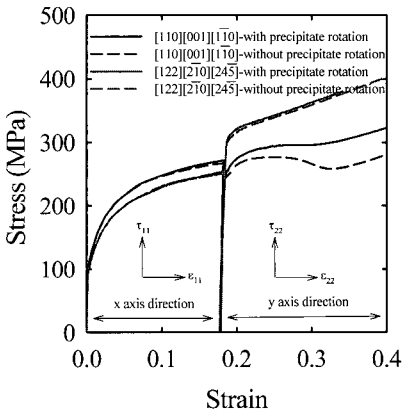

Fig. 9 Stress-strain curves ($\tau_{11}-\varepsilon_{11}$ and $\tau_{22}-\varepsilon_{22}$) in [110][001][1 $\bar{1}$0] and [122][2 $\bar{1}$0][24$\bar{5}$] crystalline orientations with load path change

5. Conclusions

The effect of the thin precipitates on the anisotropy of the initial slip resistance and isotropic-kinematic hardening has been modeled in this article. From the results of the numerical simulation it is found that the suggested model represents the initial plastic anisotropy at least qualitatively well and that it has an improved representation of various characteristic hardening behaviors in comparison with conventional hardening descriptions where the precipitate structure is not reflected.

Acknowledgement

This work was supported by the Ministry of Science and Technology through the National Research Laboratory of Korea.

References

[1] W. F. Hosford, R. H. Zeisloft, 1972, The anisotropy of age-hardened Al-4 Pct Cu single crystals during plane-strain compression, Metall. Trans., Vol. 3, pp. 113~121.

[2] P. Bate, W. T. Roberts, D. V. Wilson, 1981, The plastic anisotropy of two-phase aluminum alloys-I. Anisotropy in unidirectional deformation, Acta Metal., Vol. 29, pp. 1797~1814.

[3] Sung Ho Kim, B. J. Song, Woo Seog Ryu, 2001, The effect of W and N addition on the mechanical properties of 10Cr steels, Metals and Materials International, Vol. 7, pp. 297~302.

[4] A. W. Zhu, J. Chen, E. A. Starke Jr., 2000, Precipitation strengthening of stress-aged Al-xCu alloys, Acta. Mat., Vol. 48, pp. 2239~2246.

[5] ABAQUS, 2002, ABAQUS, Reference Manuals. Hibbit, Karlsson, Sorensen, Inc.

[6] Chung-Souk Han, R. H. Wagoner, F. Barlat, On precipitate induced hardening in crystal plasticity: algorithms and simulations, Int. J. Plasticity, Vol. 20, pp. 1441~1461.

[7] Y. W. Chang, R. J. Asaro, 1981, An experimental study of shear localization in aluminum-copper single crystals, Acta Metal., Vol. 29, pp. 241~257.

[8] R. Becker, J. F. Butler, H. Hu, L. A. Lalli, 1991, Analysis of an aluminum single-crystal with unstable initial orientation (001)[110] in channel die compression, Metal. Trans. A, Vol. 22, pp. 45~58.